

Spatial transcriptomics links hepatocytemacrophage interactions to viral signatures in seronegative hepatitis

Amber Bozward

a.g.bozward@bham.ac.uk

University of Birmingham https://orcid.org/0000-0001-6637-8952

Mahboobeh Buhruznia

University of Birmingham

John Cole

University of Glasgow

Scott Davies

University of Birmingham

Kylie Savoye

University of Birmingham https://orcid.org/0009-0008-0111-8541

Chiranjit Das

University of Birmingham

Matthew Pugh

University of Birmingham https://orcid.org/0000-0002-6324-661X

Grace Wootton

University of Birmingham https://orcid.org/0009-0005-7641-8053

Patricia Reis Nisa

University of Birmingham

Fabian Spill

School of Mathematics, University of Birmingham, Edgbaston https://orcid.org/0000-0001-8462-5080

Owen Cain

Queen Elizabeth Hospital

Adam Croft

University of Birmingham https://orcid.org/0000-0002-9487-0511

Alan McNally

University of Birmingham https://orcid.org/0000-0002-3099-630X

Ye Oo

University of Birmingham https://orcid.org/0000-0002-0495-6734

Article

Keywords: Autoimmune hepatitis, seronegative hepatitis, spatial transcriptome, meta-transcriptome, CD63, macrophage, virus, TNF receptor superfamily

Posted Date: November 11th, 2025

DOI: https://doi.org/10.21203/rs.3.rs-7971511/v1

License: © ① This work is licensed under a Creative Commons Attribution 4.0 International License. Read Full License

Additional Declarations: There is **NO** Competing Interest.

Spatial transcriptomics links hepatocyte-macrophage interactions to viral signatures in seronegative hepatitis

Amber G. Bozward^{1,2,3,9*}, Mahboobeh Behruznia⁴, John Cole⁵, Scott P. Davies^{1,2}, Kylie Savoye⁶, Chiranjit Das^{1,2}, Matthew Pugh¹, Grace Wootton¹, Patricia Reis Nisa⁷, Fabian Spill⁶, Owen Cain⁸, Adam P. Croft^{7,9}, Alan McNally⁴, Ye H. Oo^{1,2,3,9,10}

¹Department of Immunology and Immunotherapy, School of Infection, Inflammation and Immunology, College of Medicine and Health, University of Birmingham, Birmingham, United Kingdom

²Centre for Liver Research, University of Birmingham and University Hospital Birmingham NHS Foundation Trust, Birmingham, UK

³Centre for Rare Diseases, European Reference Network on Hepatological Diseases (ERN-RARE-LIVER) centre, Birmingham, UK

⁴Department of Microbes, Infection and Microbiome, School of Infection, Inflammation and Immunology, College of Medicine and Health, University of Birmingham, Birmingham, United Kingdom

⁵University of Glasgow, Bioinformatics facility, Glasgow, UK

⁶School of Mathematics, College of Engineering and Physical Sciences, University of Birmingham, UK

⁷Rheumatology Research Group, Department of Inflammation and Ageing, College of Medicine and Health, University of Birmingham, Birmingham, UK.

⁸Pathology department, Liver Unit, Queen Elizabeth Hospital, Birmingham, UK

⁹National Institute for Health and Care Research (NIHR) Birmingham Biomedical Research Centre, UK

¹⁰Liver Transplant and Hepatobiliary Unit, Queen Elizabeth Hospital, UHB NHS Foundation Trust, Birmingham, UK

Corresponding authors(*):

Dr Amber G. Bozward - a.g.bozward@bham.ac.uk;

Professor Ye H. Oo - <u>y.h.oo@bham.ac.uk</u>

Keywords: Autoimmune hepatitis, seronegative hepatitis, spatial transcriptome, metatranscriptome, CD63, macrophage, virus, TNF receptor superfamily

Conflict of interest statement: The authors have nothing to declare.

Author contributions

AGB – Conception and design of the project, performed experiments, analysis and interpretation of the project, writing and editing the manuscript

MB – Analysis of RNA meta-transcriptomics data

JC - Helped performed analysis of Visium and CosMx data

SPD – IHC staining and Visium imaging

KS – Figure creation and bioinformatics

CD - Figure creation and bioinformatics

MP - HERVK staining and imaging, immunohistochemistry expert advice

GW – Assisted Visium experiments

PRN – Cut samples on the Visium slides, and cut tissue for RNA extraction

FS – Bioinformatics and intellectual input

OC – Identified seronegative and AIH samples and immunohistochemistry expert advice

APC – Advice for Visium, manuscript editing

AM – Substantial intellectual input, meta-transcriptomics analysis, manuscript editing

YHO – Conception and design of the project, writing and editing manuscript and supervised the project.

Acknowledgements

The authors are grateful to the patients and donors at the Queen Elizabeth Hospital, Birmingham, UK, allowing us to use research samples with consent. We would like to thank the hepatology department clinical and nursing staff who helped us with samples allocation and patient' recruitment. Additionally, we thank the NHS team of Daniel Kearns, Kulvinder Gill and Janine Fear for their continued efforts in managing sample access with established ethics at the Centre for Liver and Gastrointestinal Research. The authors also thank Joe Flint & Dr David Gardner from Birmingham Tissue Analytics for providing assistance with the CosMx service platform and also Professor Andrew Beggs and Dr Anetta Ptasinska from University of Birmingham Genomics Facility for aiding with the 10X Visium sequencing. The authors also acknowledge the University Microscope facility for the help with microscopy work.

K.S. thanks the Centre for Doctoral Training in Topological Design, the Engineering and Physical Sciences Research Council (EPSRC), and AstraZeneca (grant no. EP/S02297X/1 to K.S.) for funding this research.

F.S. is supported by a UKRI Future Leaders Fellowship (grant no. MR/T043571/1).

A.P.C. is supported by a Kennedy Trust for Rheumatology Research Senior Research

Fellowship (KENN 19 20 06), Foundation for Rheumatology Research Career grant

(FOREUM; Project 038), Versus Arthritis grants 23153, 22710, MRC grant MR/W028557/1.

M.B. and A.M. were funded by the National Institute for Health and Care Research (NIHR)

Birmingham Biomedical Research Centre - NIHR203326

A.G.B. & Y.H.O. are supported by Wellcome Trust Discovery award (reference:

326757/Z/25/Z), Sir Jules Thorn Charitable Trust (reference: 18JTA), Whitney wood

Scholarship awarded by the Royal College of Physicians and University Hospital

Birmingham Charity.

ABSTRACT 200/200

Background:

Seronegative hepatitis (SNH) is an acute fulminant liver injury which leads to liver failure, requiring urgent transplantation. Its clinical, biochemical, and histological features mimic autoimmune hepatitis (AIH). SNH aetiology and pathogenesis is unknown thus defining triggers and immune pathways is essential for timely diagnosis and effective treatment.

Methods:

We applied multi-modal spatial transcriptomics, combining CosMx[™] single-cell resolution with Visium whole-transcriptome profiling, to SNH, AIH and healthy donor explant liver tissue. Data were integrated with meta-transcriptomics and multiplex imaging on the same tissues to identify disease-specific signatures.

Results:

SNH livers displayed a significant expansion of macrophages enriched for interferon-stimulated genes (*MX1*, *ISG15*, *OAS1*, *IFIT3*), compared to AIH. MX1⁺ hepatocytes were also uniquely expanded in SNH. Meta-transcriptomic profiling of matched livers revealed transcriptional upregulation of human endogenous retroviruses (HERVs), including HERV-K, in SNH and AIH livers but absent in donor livers. HERV-K protein was detected in SNH by tissue staining, implicating viral aetiology as a potential immune trigger. Furthermore, SNH was distinguished by CD63 upregulation and selective activation of the LIGHT-HVEM pathway between macrophages and hepatocytes.

Conclusions:

Multi-modal spatial profiling reveals that SNH is transcriptionally and immunologically distinct from classical AIH, with evidence for viral-associated immune activation driving severe liver injury.

INTRODUCTION

Autoimmune hepatitis (AIH) is an immune-mediated liver disease driven by an aberrant attack on hepatic tissue by the host's innate and adaptive immune systems, with unknown aetiology^{1,2}. It is typically diagnosed based on characteristic clinical presentation with jaundice, abnormal liver enzymes and immune mediated hepatitis histological findings in the presence of circulating autoantibodies³. Seronegative hepatitis (SNH), sometimes referred to as autoantibody-negative AIH, is a form of acute immune-mediated liver injury that closely resembles and shares many clinical, biochemical and histopathological features with classical AIH, however autoantibodies are absent⁴. However, a unique feature of SNH is an overwhelming acute fulminant hepatitis leading to pan-acinar hepatocyte necrosis which leads to liver failure.

It is still unknown whether SNH represents a distinct immune-mediated liver disease from a precipitating trigger or is it an early onset of AIH before autoantibodies can be synthesised⁵⁻⁷. Presentation of SNH is normally in young adults with features of fulminant hepatic failure^{8,9}. In many cases, SNH progresses rapidly leading to massive liver necrosis with poor outcomes. Liver transplantation is the only life-saving definitive treatment¹⁰ and the majority of patients will not survive unless they undergo an urgent liver transplantation.

In this study, we comprehensively profile gene, metagenome, transcriptome and protein expression on liver tissue from rare samples of SNH patients, AlH patients, and donor controls by combination of CosMx[™] single-cell spatial transcriptomics, Visium whole-transcriptome, meta-transcriptomic, immunohistochemistry and confocal microscopy. Crucially, and a unique feature in this study, the same patient samples were used across all modalities, allowing direct integration of spatial, transcriptional, immune pathways and protein-level data on hepatocytes and intrahepatic immune cells. This multi-OMICs platform

approach enabled us to identify cellular and molecular features unique to SNH and allowed us to dissect the aetiology and pathogenesis pathway with these precious samples.

Excitingly, we found an antiviral signature which is associated with hepatic macrophages (Kupffer cells), transcriptional upregulation of endogenous retroviruses (HERVs) along with LIGHT-HVEM (also known as TNFSF14-TNFRSF14) signalling pathway in SNH. Our data reveals that SNH is characterised by a distinct spatial immune microenvironment, possibly triggered by exposing antiviral gene expression programs by the host immune response, and subsequent activation of TNF receptor superfamily-related immune cells—parenchyma communication networks. These findings redefine the description of SNH as a mechanistically distinct immune mediated liver disease with implications for potential new diagnosis tools and the development of potential future therapy.

METHODS

Ethical approval

All human samples were obtained from surgical procedures carried out at the Queen Elizabeth Hospital, Birmingham, UK, with written consent from patients. Ethical approval for the study was granted by the Local Research Ethics Committee at the University of Birmingham (REC; reference number 18/WA/0214, IRAS reference 223072). Diseased liver tissue was sourced from explanted livers from patients undergoing transplantation. Donor livers were received in cases where the liver was rejected for transplantation or surplus to clinical requirements.

CosMx data generation

FFPE explant liver samples were processed using the Human Universal Cell Characterisation 1000-plex panel¹¹ following the manufacturer's protocol (Item number:121500005, Bruker Spatial Biology, Seattle, WA). Briefly, tissue sections were cut to a thickness of 5um and mounted on Superfrost Plus Micro Slides within a 15 mm x 20 mm imaging area and baked overnight at 60°C to enhance adherence. After deparaffinisation, target retrieval was performed, followed by permeabilization. Fiducial markers were applied for precise image alignment, followed by post-fixation and blocking. Slides were then hybridized overnight with RNA-specific probes from the 1000-plex RNA panel. DAPI was stained for nuclear visualisation and cell segmentation markers CD298/Beta-2-Microglobulin (B2M), CK8/18, and CD45 were applied. The prepared slides were loaded into the CosMx SMI instrument for imaging. Regions of interest were selected for imaging and processed using the fully automated, on instrument analysis pipeline. The raw images were processed and decoded using the AtoMx™ Spatial Informatics Platform (SIP) (v1.3.2). Segmentation was performed using AtoMx built-in cellpose algorithm. Cell segmentation was generated using cellpose on the AtoMx software using the non-neuronal cell profile. To ensure we were

using the optimal segmentation methodology, the small and large cell AtoMx segmenting profile was tested as well as the addition of Baysor segmentation which did not improve the segmentation.

CosMx data processing and analysis

The dataset was segmented under default settings using AtomMx and exported as flat text files. The dataset was loaded into R (4.5.1) using Seurat (5.1.0)¹² and cells were assigned to the appropriate samples and conditions based on FOV. The relationship between per cell feature counts, number of features, and sample was assessed using FeatureScatter, VInPlot, and SpatialFeaturePlot (Supplementary Fig. 1A-C). Indicating high consistency between sample quality, despite some samples having low cell counts due to tissue size (Supplementary Fig. 1C).

Next, the data was normalised using SCT and PCA performed. The elbow plot (Supplementary Fig. 1D) suggested between 10-15 dimensions were potentially informative. 15 dimensions were carried forward. Clustering was performed using FindNeighbors and FindClusters under default settings and a UMAP generated (Supplementary Fig. 1E), which showed a clear per sample batch effect. The PCA was integrated on sample using Harmony (3.8)¹³, under default settings. The integrated PCA was re-clustered and the UMAP generated which displayed high consistency between samples (Supplementary Fig. 1F).

To identify cell types, per cluster were identified using FindAllMarkers specifying only.pos = TRUE, min.pct = 0.25 and logfc.threshold = 0.25. SingleR (2.1)¹⁴ with the Human Primary Cell Atlas database was used as a prior, with clusters manually curated based on the markers and spatial information (Supplementary Table 1). Due to the limited markers in the 1k plex assay, assigning immune cell types with high resolution proved challenging. To improve marker resolution, we identified cells as "immune" and "non-immune" and subsetted the dataset, then re-ran the PCA, integration, clustering and find FindAllMarkers on each subset

(Supplementary Table 2 and 3 respectively). Manual curation of the subsetted markers resulted in the identification of 12 cell types.

CosMx spatial region classification: parenchyma and non-parenchyma

To separate parenchyma (P) and non-parenchyma (NP) cells, a custom Python script was used to dynamically select spatial niches based on histology. Regin boundaries were manually drawn, with validation against known cell-type markers (Supplementary Fig. 2). Next differential expression analysis was performed between conditions, for P or NP, for each cell type. To do so, we collapsed the data into pseudo counts by sample + cell type + P / NP, using AggregateExpression. We removed any sample with < 50,000 reads, and pairwise differential expression was calculated using DESeq2 (1.48.1) under default settings. The results were visualized using Searchlight (2.0.3) specifying p.adj < 0.05, absolute log2fold > 1 for significance, and using the String (11.5) and TRRUST (2.0) databases.

Visium data generation

The Visium spatial transcriptomics data was generated following the Visium spatial transcriptomics platform user guide (10X Genomics, CG000239 Rev B). Briefly, the Visium workflow began with sectioning 10um fresh frozen explant liver tissue onto a Visium RNA capture slides. The tissue was fixed, H&E stained and imaged without a cover slip using a slide scanner (Axio Scan, Zeiss). Permeabilization was then preformed to make the mRNA accessible, permeabilization time ranged between 6-12 min depending on the samples determined using tissue optimisation slides and reagents (10X Genomics). Tissue sections were incubated in permeabilization buffer and then reverse transcription, second strand synthesis and denaturation, complementary DNA (cDNA) amplification, and quality control were performed to ensure proper construction of spatial gene expression libraries (10X Genomics). High-throughput sequencing was performed on a NovaSeq sequencer (Illumina)

using a SP 200 cycle flow cell to achieve recommended sequencing depth. Sequencing reads were demultiplexed and aligned to the human genome (GRCh38-2020-A) using Space Ranger (v.2.1.0; 10X Genomics). All data analysis and visualizations were conducted in R (v4.5.1).

Visium gene deconvolution and enumeration of cell fractions by CIBERSORTx

Published scRNA-seq data from donor livers containing parenchymal and non-parenchymal cells (n=8444 total cells)¹⁵ was used to generate CIBERSORTx "signature matrix" files (https://cibersortx.stanford.edu)¹⁶. Signature matrices contained gene profiles of hepatocytes, hepatic stellate cells, portal endothelial cells, plasma cells, B cells, NK cells, inflammatory and non-inflammatory macrophages, T cells, cholangiocytes and central venous LSECs. Next, average gene expression (median-normalised) of parenchymal and non-parenchymal areas were converted into CIBERSORTx "mixture" files containing differential gene expression values measured by spatial transcriptomics. The mixture file and the signature matrices were uploaded and run in the "impute cell fractions" module of CIBERSORTx¹⁷.

Visium data processing and analysis

Visium Spatial Gene Expression data (10x Genomics) were processed using the Space Ranger pipeline (v2.1.0) with the GRCh38 human genome reference for alignment and gene quantification. Tissue sections were quality-checked using H&E staining and imaged prior to permeabilisation and library preparation. The resulting dataset was loaded into R (4.5.1) using Seurat (5.1.0), and the relationship between per cell feature counts, number of features, and sample was assessed using FeatureScatter, VlnPlot, and SpatialFeaturePlot (Supplementary Fig. 3A-C). The results showed inconsistency between the counts observed in each sample, with two samples (AH_1607 and AH_7538) showing very low counts. For all samples the expected relationship between counts and features was observed (Supplementary Fig. 3C),

suggesting no issue with the library preparation, and the most likely cause was tissue adherence to the slides. All samples were taken forward to improve reduction, clustering and cell type identification, however several samples were filtered out at the pseudo-bulk step. Next, the data was normalised using SCT, and PCA and UMAP performed. The initial UMAP showed a clear per sample batch effect (Supplementary Fig. 3D). The data was integrated using Seurats FindIntegrationAnchors function. With 3,000 integration markers and samples AH_2709 and SN_3303 used as the reference. The integrated data was then re-normalised using SCT, and PCA performed. The PCA suggested between 10 and 20 dimensions were potentially informative (Supplementary Fig. 3E). 15 dimensions were carried forward. Clustering was performed using FindNeighbors and FindClusters under default settings and a UMAP generated (Supplementary Fig. 3F).

The 10x loupe browser platform was used to identify regions that were either parenchyma (P), non-parenchyma (NP), deep parenchyma (DP) or deep non-parenchyma (DNP). These cell annotations were imported into the Seurat metadata. The data was collapsed into pseudo counts by sample + region (P, NP, DP, DNP). We removed any sample with < 50,000 reads, and the data was corrected for read count using CombatSeq (SVA)¹⁸. Next, pairwise differential expression was calculated using DESeq2 (1.48.1) under default settings, and a normalised expression table produced. The results were visualized using Searchlight (2.0.3) specifying p.adj < 0.05, absolute log2fold > 1 for significance, and using the String (11.5)¹⁹ and TRRUST (2.0)²⁰ databases.

To deconvolute, the data the CibersortX web platform was used. Firstly, a signature genes file was created. The healthy donor single cell dataset (GSE115469) was imported into R, and the top 25 markers for each cell type identified using FindAllMarkers. Next, the count data was collapsed by cell type into Pseudobulk. To reduce complexity the separate hepatocyte subclusters were collapsed into one. The counts were normalised using DESEq2²¹ and then filtered to contain only the top 25 markers for each cell type. This was uploaded as the signature genes file. To generate the mixture file, Visium pseudo bulk normalised expression table was filtered to contain only genes in the signatures gene file.

Neighbourhood enrichment analysis

To investigate the spatial organisation of cells, we used SquidPy (Python; v3.10.18; Squidpy v1.6.5; Scanpy v1.11.13)²². Spatial neighbourhood graphs were generated with the squidpy.gr.spatial_neighbors function, connecting cells within a specified radius. After systemically testing different radii, we determined that 50 µm was the optimal radius to use.

Neighbourhood enrichment analysis was then performed on these graphs using squidpy.gr.nhood_enrichment, which compares observed co-occurrence of cell type labels to a permutation-based null distribution (1,000 shuffles). This produced Z-scores describing enrichment (positive values) or depletion (negative values) for each label pair. Scores were calculated per sample and averaged within disease groups.

We also computed Ripley's G statistic²³ to assess spatial segregation or mixing of each cell type. For a given type i,

 $G(t)=P(di \leq t)$

where di is the distance to the nearest neighbour. Curves were averaged within each disease group.

Immunohistochemistry

All immunohistochemistry was performed using paraffin-embedded tissue cut to three micrometres onto a positively charged slide. Tissue sections were deparaffinized with xylene and rehydrated using 97% industrial denatured alcohol (IDA) and then underwent antigenretrieval procedures by microwaving in Tris-based antigen unmasking solution (Vectorlabs).

Endogenous peroxidase activity and non-specific antibody binding within tissue sections was blocked using REAL peroxidase blocking solution (Dako) and 2X casein solution (Vectorlabs), respectively. Sections were incubated with primary antibodies (Supplementary Table 4) at room temperature for 1 h or overnight at 4°C depending on the antibodies used. Appropriate isotype-matched controls were used to stain serially cut tissue sections for all procedures. For chromagen-based detection, slides were washed with TBST, and then primary antibodies were detected using anti-rabbit or anti-mouse HRP-conjugated secondary reagents (Vectorlabs). IMMPACT DAB (Vectorlabs) was used as a chromogen for stain development. Sections were counterstained with Mayers Haematoxylin which was developed using hot water. Sections were washed in water, dehydrated with 97% IDA and xylene, and then mounted with DPX mountant (CellPath)²⁴. Sections were then scanned using a Zeiss Axio Scan.Z1 slide scanner.

For immunofluorescence, sections were washed as above and then incubated with appropriate, fluorophore-tagged secondary antibodies, diluted in 2X casein buffer, for 1 h. Sections were then incubated with TBST containing 1 µg/ml Hoechst 33342 (Life Technologies) for 10 min. Autofluorescence was then quenched in sections using TrueView (Vectorlabs). Sections were washed and then mounted on to glass coverslips using Vectorshield plus (Vectorlabs). Sections were then imaged using a Zeiss 880 LSM confocal microscope piloted by Zen black v2.3 software. Where consecutive round multiplexing was necessary – when using multiple rabbit antibodies – coverslips were removed, and sections were treated with Vectorplex (Vectorlabs) as per manufacturer's instructions. Samples were then blocked in 2X3.12 casein buffer as above and then staining procedures were repeated. Previous imaging positions were recalled using the Zen black v2.3 software and images were overlaid using Zen lite v3.12.

Further details of chromogen-based immunohistochemistry methods can be found in Davies *et al* ²⁵. Details of fluorescence immunohistochemistry methods can be found in Davies *et al* ²⁴

Quantifying DAB staining with QuPath

Using QuPath (version 5.1), DAB staining was quantified in digital slide images (Supplementary Fig. 4). Initially, the images were opened in QuPath with the image type set to Brightfield (H-DAB). Stain vectors for Haematoxylin and DAB were optimised to ensure accurate colour separation. The whole tissue section was selected using the annotation tools. Colour deconvolution was then performed using the estimate stain vectors function to separate Haematoxylin and DAB channels.

Positive cell detection algorithms were configured and executed to identify DAB-stained cells, with adjustments made for nucleus and cytoplasm detection as well as positivity thresholds. Detected cells underwent review, and parameters were fine-tuned to ensure accuracy. Quantification results were accessed in the measurement table and exported for subsequent analysis.

RNA extraction

RNA was extracted to check the RIN values of the tissues used for spatial transcriptomics and also for the meta-transcriptomics analysis.

Ten scrolls of 10mm thick cryosections cut from each frozen liver tissue block were placed into an Eppendorf for RNA extraction using the Qiagen RNeasy Mini kit, following the protocol suggested by the manufacturer.

Meta-transcriptomics

RNA extracted from frozen liver blocks was submitted to Novogene for meta-transriptomics sequencing. Ribosomal RNA was depleted from the total RNA, which was then reverse transcribed into cDNA. Libraries were prepared and sequences using high-throughput Illumina technology (n=5 AIH, n=6 SN, n=4 donor).

Barcode trimming and quality control were performed using fastp v 0.23.4 ²⁶ to discard reads shorter than 40 nucleotides and a Phred quality score of ≥Q20. Reads were then aligned to the human genome (GRCh38) using Bowtie2 v 2.5.4 (--very-sensitive-local -k 100 --scoremin L, 0, 1.6 for multi-mappings) ^{27,28}. The Bowtie2 output was used in the Telescope v 1.0.3 to quantify accurate retrotransposon expression on samples using HERV and L1 annotation (retro.hg38.v1, available on

https://github.com/mlbendall/telescope_annotation_db/tree/master/builds, accessed on 3 January 2025). Host gene quantification was performed using Salmon v 1.10.3 ²⁹ through Ensembl GRCh38 genome assembly and annotation. Telescope and Salmon outputs were used to calculate retrotransposons differentially expressed in SN and AlH vs donor samples using DESeq2 ³⁰. Retrotransposons with p.adj-values < 0.05 and absolute (log2fold) > 1were considered differentially expressed and visualised using Volcano plots with Bioconductor EnhancedVolcano package.

Statistical analysis

Statistical analysis were performed using either Student's t-tests or Mann-Whitney tests, selected based on data distribution assessed by the Kolmogorov-Smirnov test. Data presented are represented as mean \pm SEM, with horizontal bars indicating the median. When comparing mean values generated between experimental groups, differences were considered significant if p<0.05. GraphPad Prism V10 was used for statistical analysis. GraphPad Prism V10 and RStudio V10.10.0 were used for figure generation.

RESULTS

Exploring spatial gene signatures of immune cells and hepatic parenchyma in autoimmune hepatitis and seronegative hepatitis liver tissues

To investigate the immune mediated hepatitis pathogenesis through gene signatures, we performed spatial transcriptomics on human explant liver tissues from seronegative hepatitis (SNH) and autoimmune hepatitis (AIH) patients and compare with donor liver tissues as control (Fig. 1A). Same patients' samples were used throughout the study across all platforms, including CosMx spatial transcriptomics, Visium whole-transcriptome profiling, meta-transcriptomics, immunohistochemistry (IHC), and confocal microscopy enabling robust multimodal validation across matched liver tissue sections. Clinical characteristics were comparable across SNH, AIH and donors (Fig. 1B).

Firstly, we performed spatial transcriptomics using the CosMx Spatial Molecular Imager on eight liver samples (3 SNH, 2 AIH, 3 donors) and subsequently selected 951 fields of view (FOVs) (Supplementary Fig. 5). All liver tissues contain areas of both parenchyma and non-parenchyma, capturing a total of 989,651 individual cells. Unsupervised clustering using the Leiden algorithm was applied to gene expression data, and clusters were annotated into 13 distinct cell types based on canonical marker genes (Fig. 1C, Supplementary Fig. 6A-C). Further sub-clustering of selected cell types includes macrophages, B cells, T cells, and hepatocytes which allow increased resolution of key immune and parenchymal populations in hepatic lobules (Fig. 1C, Supplementary Fig. 6D-K). Spatial resolution was inherently limited to 1,000-gene targeted transcriptome CosMx panel. To visualise the spatial organisation of these annotated cell types within hepatic lobules, we overlaid the cell-type cluster map with the corresponding immunofluorescence images, revealing distinct localisation patterns of immune cells across tissue compartments (Fig. 1D).

Hepatic macrophages are significantly upregulated in seronegative hepatitis and express viral related markers

To quantify changes in the liver immune microenvironment, we analysed cell-type proportions across the three cohorts using CosMx spatial transcriptome. As expected, hepatocytes were the most abundant cell type in all groups (Fig. 2A).

To spatially contextualise these changes, we developed a custom annotation workflow in Python—guided by an expert consultant liver pathologist—to manually delineate parenchymal and non-parenchymal regions across all CosMx images (Supplementary Fig. 2). This approach enabled anatomically accurate classification of liver compartments for downstream spatial analyses. In non-parenchymal regions, SNH samples displayed a significant increase in the proportion of hepatic macrophages (Kupffer cells) compared to AlH and donor livers (Fig. 2B; p < 0.05), indicating a selective enrichment of these cells in the inflamed microenvironment of SNH livers (Fig. 2C). By contrast, donor samples showed a significantly higher proportion of hepatocytes in parenchymal regions (Supplementary Fig. 7A-B), consistent with preserved architecture and reduced parenchymal injury. Ripley's G analysis showed overlapping curves for parenchymal and non-parenchymal areas in SNH samples indicating similar spatial mixing, whereas in AlH and donor samples the curves were clearly separated, reflecting distinct spatial organisation (Supplementary Fig. 7C).

To investigate whether hepatic macrophages (Kupffer cells) in SNH patients exhibit distinct transcriptional profiles, we subclustered CosMx-identified hepatic macrophages into six subsets based on differential gene expression: anti-inflammatory, *APOC1*^{hi}, *LYZ* ^{hi}, Mregs, pro-inflammatory, and *THBS1*^{hi} macrophages (Supplementary Fig. 7D). The relative frequencies of these macrophage subsets were comparable across SNH, AIH, and donor samples indicating that differences in hepatic macrophage are related to transcriptional changes rather than altered subset composition.

Notably, hepatic macrophages in SNH samples showed consistent upregulation of multiple interferon-stimulated genes (ISGs), including MX1, OAS1, OAS2, ISG15, IFIT3 and IFI44L (Fig. 2D). These genes are canonical markers of antiviral response and were significantly enriched in SNH compared to both AlH and donor livers (Fig. 2E; p < 0.05) and showed upregulation of these markers in hepatic macrophages (Supplementary Fig. 7E).

We selected *MX1*, *ISG15*, *OAS2* and first, we showed molecule expression of these markers on the spatial map (Fig. 2F). To validate these findings at the protein level, we used matched patients' samples demonstrating the expression of *MX1* on macrophages in SNH patients using immunofluorescent imaging (Fig. 2G) as well as the expression of *ISG15* and *OAS2* comparing between SNH, AIH and donor samples confirming increased protein expression in SNH tissues compared to AIH and donor controls (Fig. 2H).

Furthermore, antiviral gene expression levels significantly correlated with total bilirubin concentrations in SNH patients (Fig. 2I, Supplementary Fig. 8A), suggesting a potential link between innate immune cells: macrophage activation and extensive necrotic liver injury.

Seronegative hepatitis is characterised by pronounced hepatic macrophage clustering and macrophage-centred immune neighbourhoods

To investigate the spatial organisation of immune and parenchymal cells in SNH liver disease, we first assessed clustering within individual cell types using Ripley's G function. Compared with random expectation, multiple immune cell types, including macrophages, T cells, B cells and monocytes, demonstrated significant clustering patterns in SNH livers, indicating that these populations preferentially aggregate rather than distribute randomly (Fig. 3A, Supplementary Fig. 8B-C). We next quantified neighbourhood enrichment to evaluate preferential cell-cell co-localisation. Across SNH samples, the strongest co-

localised enrichment was observed between hepatic macrophages and other cell types, including macrophages-macrophages, macrophages-T cells and macrophages-monocytes pairs (Fig. 3B). These hepatic macrophage-centred co-localisations consistently rank among the most enriched neighbourhoods. In contrast, the strongest co-localisation did not include macrophages in AIH and donor cohorts (Supplementary Fig. 9A-B). Direct comparison across disease groups confirmed that hepatic macrophage increased colocalization with other hepatic macrophages, T cells and monocytes and this is a distinguishing feature of SNH tissue (Fig. 3C). Macrophage-Hepatocyte co-localisation was significantly reduced in SNH samples, suggesting disruption of homeostatic immune-parenchymal interactions and a shift towards immune-immune clustering such as macrophage-T cells.

Furthermore, global differential neighbourhood enrichment analysis further highlighted the specificity of macrophage-driven spatial immune crosstalk networks in SNH. Compared with donor tissue, SNH demonstrated strong enrichment of macrophage-macrophage enrichment (Fig. 3D, top, Supplementary Fig. 9C-D). This was also highlighted in SNH compared to AlH samples (Fig. 3D, bottom). Together, these findings demonstrate that SNH is characterised by pronounced macrophage clustering and macrophage-centred immune neighbourhoods, distinguishing it from both AlH and donor liver tissue.

MX1⁺hepatocytes are significantly expressed in seronegative hepatitis

Sub-clustering hepatocytes revealed distinct hepatocyte subsets defined by stress and antiviral signatures, including $MX1^+$, $IGFBP7^+/SPINK1^+$, and $INSR^+$ populations, which were disproportionately expanded in SNH compared with AlH and donor tissue (Fig. 3E). Due to $MX1^+$ hepatocytes being significantly increased in SNH with minimal expression in AlH and donor samples (Fig. 3F), and to the increased expression of MX1 on macrophages in SNH samples, we showed localisation of MX1 transcripts in hepatocytes of SNH patients (Fig. 3G) and validated this finding with immunofluorescence staining on matched SNH liver

tissues demonstrating co-localisation of MX1 protein with the hepatocyte marker ASGR1 (Fig. 3H).

Non-parenchyma region of seronegative hepatitis are enriched with viral response signatures

To complement the high-resolution CosMx findings and capture comprehensive transcriptomic changes, we applied the 10X Genomics Visium spatial transcriptomics platform to liver tissues from same patients (SNH=6, AIH=5). H&E staining and expert pathological annotation delineated parenchymal and non-parenchymal regions, including fibrotic and portal areas (Fig. 4A, Supplementary Fig. 10A-C).

Due to the 55 µm spot size, some Visium spots contained mixed tissue compartments. To ensure spatial specificity, we defined "deep parenchyma" and "deep non-parenchyma" by selecting spots located at least two barcodes away from boundaries (Fig. 4A). Unsupervised clustering and UMAP projection confirmed distinct gene expression profiles separating parenchymal and non-parenchymal compartments (Fig. 4B, Supplementary Fig. 10D-G).

Cell-type deconvolution using integrated liver scRNAseq references identified 11 major intrahepatic cell types with broadly similar frequencies between SNH and AlH, with the exception for an increase in non-inflammatory macrophages specifically within the SNH deep parenchyma (Supplementary Fig. 11A–D).

Importantly, differential gene expression analysis revealed a pronounced signatures associating host response to virus which is predominantly enriched in SNH non-parenchymal areas, characterized by upregulation of genes involved in viral processing, immune cell death, and tissue regeneration (Fig. 4C). In contrast, AlH non-parenchyma exhibited gene signatures associated with cell-cell signalling, immunometabolism, and coagulation inhibition

typical of end-stage liver disease as expected by disease pathology (Supplementary Fig. 11E), AIH parenchyma did not have enough pathways to form a network (Supplementary Fig. 11F).

In parenchymal areas of SNH livers, pathways related to antigen presentation, innate and adaptive immune activation (including NK and B cells), and macrophage migration were enriched, reflecting an active immune microenvironment within hepatocyte-rich zones (Fig. 4D).

Together, these data demonstrate that liver parenchymal and non-parenchymal compartments possess unique transcriptomic profiles, with a specific enrichment of viral processing pathways and host response to virus in the non-parenchymal regions of SNH livers, highlighting a compartmentalised antiviral immune response that distinguishes SNH from AIH pathology.

CD63 is selectively upregulated in seronegative hepatitis liver tissue and localised to hepatic macrophages

To identify spatially relevant genes differentiating SNH and AIH, we performed differential expression analysis using Visium spatial transcriptomics in both parenchymal and non-parenchymal regions. Our analysis showed *CD63*, *MMP12*, *HM13*, and *C1QA* genes were significantly upregulated in SNH compared to AIH across both tissue compartments (Fig. 5A-B; Supplementary Fig. 12A-B).

To validate these findings at the protein level, we performed immunohistochemical staining on matched FFPE samples from the same patients' liver tisse from SNH, AIH and donor livers. CD63 molecule showed significantly increased staining intensity in SNH liver samples compared to all other groups (Fig. 5C-D). In contrast, MMP12 was upregulated in both SNH

and AIH compared to donor tissue, while HM13 and C1QA did not show significant protein-level differences (Supplementary Fig. 12C-D). Quantification was performed using QuPath, with automated detection and intensity scoring across matched tissue regions.

Applying our CosMx data set, we visualised the distribution of *CD63* expression across annotated cell types. Notably, *CD63* expression in macrophages was strongest and most consistent in SNH samples (Fig. 5E). To evaluate whether *CD63* expression was disease-specific, we examined publicly available single-cell RNA-seq data of liver mononuclear phagocytes (https://shiny.igc.ed.ac.uk/7efa5350ba94425388e47ea7cdd5aa64/). *CD63* expression was minimal in healthy and acetaminophen (APAP) overdose livers, but consistently observed in Non-A, Non-E (seronegative) liver disease, supporting its relevance to SNH pathology (Fig. 5F).

Meta-transcriptomics analysis reveals transcriptionally active HERVs in seronegative hepatitis and autoimmune hepatitis livers

To further elucidate the viral gene signatures observed in SNH patients, we performed metatranscriptomic analysis on same patients matched livers RNA samples from SNH (n = 6), AIH (n = 5), and donor liver tissues (n = 4). This approach enabled unbiased detection of transposable element (TE) activity, including human endogenous retroviruses. We detected the transcripts of human endogenous retrovirus (HERV), which is expressed in the germline in all SNH and AIH samples, but they were absent in donor livers, supporting the disease specificity of HERV activation. In SNH, we identified nine differentially expressed TEs (seven upregulated, two downregulated), the majority of which were HERV elements. These included HERVH_1q32.1a/b, HERVK14C_1q32.1, HERVW_1q32.1, HML1_1q32.1, and HML3_1q32.1b, all located on chromosome 1q32.1 (Fig. 6A-B). Similarly, in AIH, 13 differentially expressed TEs were identified (nine upregulated, four downregulated), including eight HERVs and five LINE-1 (L1) elements (Fig. 6C-D). Several HERVs were shared

between AIH and SN, including HERVH_1q32.1b, HERVK14C_1q32.1, and HERVW_1q32.1, suggesting overlapping activation patterns in both SNH and AIH liver disease. Annotation with Telescope confirmed that all differentially expressed HERV loci were non-protein coding (Supplementary Table 5).

To assess whether HERV activation translated to protein expression, we performed immunohistochemistry, with an expert liver pathologist, for HERV-K Gag protein on matched FFPE tissues from same patients with SNH and AIH. Robust staining was observed by expert pathologist predominantly in SNH samples, with expression localised primarily to hepatic macrophages, while no liver tissue expression was detected in AIH and donor livers (Fig. 6E).

These findings provide direct evidence that HERV elements are transcriptionally and translationally active in SNH, but only transcriptionally in AIH liver tissues and absent in donor controls. Importantly, this HERV activation occurs alongside the upregulation of interferon-stimulated genes such as *MX1*, *OAS1*, and *ISG15* in SNH samples, suggesting a potential association between endogenous retroviral activity and the antiviral immune signature observed in these livers.

Intrahepatic immune cells and hepatic parenchyma cells interactions reveal upregulation of the LIGHT pathway in seronegative hepatitis

Thus far, our data suggested host response to virus, CD63 molecule which may relate to viral processing and hepatic macrophages are involved in SNH pathogenesis. To further dissect host response to viral response we compare cell-cell interaction to donor and AlH and donor and SNH samples. We explored cell-cell interactions within parenchymal and non-parenchymal regions defined by CosMx spatial data.

AIH livers exhibited fewer interactions overall and lower interaction signal strength in both tissue compartments (Supplementary Fig. 13A-B). Visualisation of interaction networks showed distinct differences in cell-type communication patterns between patient groups (Supplementary Fig. 13C–F).

Notably, analysis of ligand–receptor pairs revealed significant upregulation of the LIGHT (homologous to lymphotoxin, exhibits inducible expression and competes with HSV glycoprotein D for binding to herpesvirus entry mediator, a receptor expressed on T lymphocytes) pathway (*TNFSF14*–*TNFRSF14* and *TNFSF14*–*LTBR*, also known as LIGHT-HVEM (herpesvirus entry mediator) and LIGHT-LTBR (lymphotoxin beta receptor) respectively) in SNH samples compared to AlH and donor cohorts (Fig. 7A). Cross-condition comparisons demonstrated that SNH displayed the highest expression of all three genes across all cell populations (p<0.0001, Fig. 7B). To understand the cell-specific expression of *TNFSF14*, *TNFRSF14* and *LTBR* we looked across the diseases on all cell types, this showed a broad expression of *TNFSF14* and *TNFRSF14* in SNH but a lacking expression of *TNFSF14* in immune cells in AlH and donor samples (Fig. 7C-D, Supplementary Fig. 13G).

High resolution multiple immunofluorescence imaging validated expression of *TNFSF14* (LIGHT) on CD68⁺ macrophages and its counterpart co-stimulatory receptor *TNFRSF14* (HVEM) on hepatocytes in SNH samples but lacking in AlH and donor samples (Fig. 7E).

DISCUSSION

In this study, we investigate the immunopathogenesis mechanism and possible triggers of seronegative hepatitis, comparing them with autoimmune hepatitis and donor livers. A unique feature of our study is the use of the same patient samples across all experimental platforms to explore underlying pathogenesis in a robust and physiological approach. We applied high-plex spatial transcriptomics to provide an in-depth spatial and transcriptional comparison, integrating CosMx single-cell spatial resolution data with Visium whole transcriptome profiling. We uncovered distinct immune signatures that highlight the unique immunopathology of SNH compared to AlH and homeostatic state of normal liver.

Our most striking finding was the significant expansion of hepatic macrophages (Kupffer cells) in SNH livers, particularly within non-parenchymal portal tract regions. The most likely explanation is pan-acinar hepatocyte necrosis in SNH, leading to collapse of the liver lobule and accumulation of hepatic macrophages around the portal regions. This finding is accompanied by an enrichment for canonical type I interferon-stimulated genes (ISGs) such as MX1, OAS1, ISG15 and IFIT3 on these macrophages. MX1 is induced by interferon, a signalling protein released by cells in response to viral infection. There is a high level of type 1 interferon in acutely inflamed liver^{31,32} such as SNH. MX1 binds to and disrupts the interaction between viral proteins, specifically basic protein 2 (PB2) and the nucleoprotein³³. Type I interferon responses are well-established mediators of antiviral immunity, typically induced during viral infections or viral mimicry states³⁴. Thus, a viral trigger may play a role in SNH, and macrophages are primed for antiviral defence, whereas in AIH T cells orchestrate an immune-mediated inflammation to autoantigens such as soluble liver antigen³⁵. The enrichment of ISGs in SNH macrophages suggests an innate immune activation that may be triggered by viral components or endogenous danger signals, similar to a previous study where macrophage-driven type I interferon signatures correlate with disease severity³⁶. Spatial analysis further revealed increased proximity of macrophagesmacrophages, macrophages-T cells and macrophages-monocytes in SNH livers, implying that disrupted tissue architecture or local microenvironmental cues may modulate macrophage activation and contribute to persistent inflammation. Hepatic macrophages are phagocytic cells in the liver and such macrophage activation states have been linked to failed resolution of inflammation and tissue damage³⁷.

Sub-massive hepatocyte necrosis or pan-acinar necrosis is a typical histology finding in SNH. Due to necrosis of parenchyma hepatocytes, we compare both parenchymal versus non-parenchymal regions. In SNH, non-parenchyma regions have accumulation of immune cells which explains liver lobule collapse leading to dense concentrations of immune cells in non-parenchyma or portal tract regions of SNH. However, this stands in contrast to acute AIH, where liver inflammation is often more spatially diffuse and the balance between injury and repair more sustainable over time. These regional patterns not only reflect the known spatial organisation of hepatic cell types but also highlight disease-specific pathophysiology. Thus, we applied spatial transcriptomic profiling using Visium which revealed marked compartmentalisation of gene expression in SNH livers, with distinct molecular programs operating in parenchymal versus non-parenchymal regions.

Non-parenchymal regions in SNH samples showed significant upregulation of genes involved in viral processing, innate immune activation, apoptosis, and cell death—signatures that align with the spatially focused on regions enriched for innate macrophages. In the parenchyma, SNH livers exhibited increased expression of genes linked to antigen presentation, cytotoxicity, and cell cycle dysregulation. These findings imply that hepatocytes in SNH are active target of tissue destruction of immune cells with attempted hepatocyte regeneration and proliferation. The enrichment of cytotoxicity and mitotic genes further suggests a dynamic but ultimately failing regenerative attempt in the face of overwhelming immune-mediated injury. Upregulation of pathways involved in macrophage migration also demonstrates that a hepatic environment of persistent inflammation and attempted

phagocytosis and repair is occurring in SNH livers³⁸. However, this regenerative response appears insufficient to counteract the extensive damage, contributing to the fulminant disease course characteristic of SNH, indicating a skewed balance toward injury as seen in acetaminophen overdose patients^{39,40}. These spatial data provide insights towards the pathogenesis of SNH suggesting that the destructive trajectory of SNH linking with viral processing and innate hepatic macrophages in necrotic and collapsed hepatocyte parenchyma.

A notable molecular distinction between SNH and AIH was the upregulation of CD63, observed at both gene and protein levels. CD63 is a member of the tetraspanin family involved in vesicle trafficking, exosome biogenesis, immune cell activation, and cell adhesion ⁴¹. Its increased expression in SNH was localised to hepatic macrophages, consistent with a heightened state of immune activation and cellular stress. Additionally, CD63 is associated with innate immune cell apoptosis 42, suggesting that its expression may also reflect clearance of apoptotic immune cells in inflamed tissue. CD63 is also prominently expressed on the surface of exosomes, and its upregulation in SNH may relate to increased intercellular signalling via CD63-enriched vesicles. These exosomes can carry microRNAs from virus that modulate local immune responses, potentially exacerbating inflammation and driving disease progression ⁴³. Importantly, CD63 plays a functional role in viral infection biology. It is enriched in late endosomes and multivesicular bodies and facilitates membrane organisation and intracellular trafficking of viruses including HIV, HPV, and influenza A virus ⁴⁴ ⁴⁵⁻⁴⁹. In addition to its role in innate immunity, CD63 has been implicated in extracellular matrix remodelling and fibrosis ⁵⁰, processes that are known to be more pronounced in SNH due to the extensive architectural disruption observed in sub-massive hepatic necrosis disease 8,51-53.

In SNH, CD63 expression coincided with robust interferon-stimulated gene signatures and active HERV transcription, suggesting a coordinated antiviral response. Importantly, CD63

upregulation distinguished SNH from AIH, reflecting stronger viral and immune-mediated inflammatory processes. Together, these findings support a model in which endogenous viral element activation, particularly pronounced in SNH, exacerbates immune dysregulation and accelerates hepatocyte inflammation and necrosis.

Complementing the macrophage-driven antiviral signature and CD63 upregulation in SNH, our meta-transcriptomic analyses detected active transcription of human endogenous retroviruses (HERVs) in both SNH and AlH liver tissues, but not in donor livers. We confirmed these findings with immunohistochemistry tissue staining on same liver tissues of SNH which we used for Visium and CosMx analysis. This finding supports the hypothesis that reactivation of endogenous retroelements may occur in inflamed human livers triggering innate immune responses including macrophages. However, HERVs signature is not seen in homeostatic state such as normal livers. The localization of HERV-K proteins to macrophages in SNH further strengthens the link between HERV expression and immune activation. Although previous studies have implicated HERV reactivation in systemic autoimmune conditions such as multiple sclerosis and lupus^{54,55} - where HERV-derived nucleic acids and proteins stimulate type I interferon pathways and contribute to chronic inflammation⁵⁶ - recent mechanistic data show that Epstein–Barr virus (EBV) infection can directly drive multiple sclerosis by expanding central nervous system-homing T-bet+CXCR3+ B cells that recruit inflammatory T cells to the brain. Thus, HERV reactivation in autoimmune contexts may represent a secondary or amplifying response to upstream initial immune triggers, such as environmental insult or viral infection, rather than the initiating cause⁵⁷.

Notably, the majority of differentially expressed HERVs in our cohort mapped to chromosome 1q32.1, a locus previously associated with autoimmunity and epigenetic dysregulation⁵⁸⁻⁶¹. While it remains unclear whether HERV activation is a cause or consequence of liver inflammation, its presence in both SNH and AIH highlights a shared

pathogenic mechanism involving viral mimicry. This data provides evidence of tissue-level HERV expression suggests that endogenous retroviral elements may contribute to sustained immune activation, adding complexity to the immunopathogenesis of SNH and AlH. This aligns with previous suggestions that viruses could play a role in triggering immune responses in genetically predisposed individuals⁶². In addition, we identified shared upregulation of five non-coding HERV loci on chromosome 1q32.1 in both SNH and AlH livers, suggesting a common mechanism of endogenous retroviral activation. Although non-coding, HERV transcripts can stimulate innate immune sensors and promote inflammation⁶³. Notably, SNH showed a broader and more dysregulated transcriptional response, particularly in macrophages, which may underlie its more aggressive clinical course.

The absence of HERV expression in donor tissue confirms the disease specificity of this signal and supports the hypothesis that HERV reactivation might be a pathological feature of both SNH and AIH. Given recent evidence from EBV-associated autoimmune diseases, it is most likely that HERV is a secondary response to unknown upstream immune stimulation, rather than a primary driver, but it remains closely associated with hepatic macrophage activation and CD63 upregulation.

We then investigate the reason for fulminant hepatocyte necrosis from aberrant immune activation in SNH. Spatial cell–cell interaction analysis revealed significant upregulation of the TNFSF14 (LIGHT)–TNFRSF14 (HVEM) signalling axes in SNH livers compared to AlH and donor tissues. We confirmed this by staining LIGHT on hepatic macrophages (Kupffer cells) and HVEM on hepatocytes in SNH. LIGHT is a member of the TNF superfamily that plays critical roles in promoting immune cell activation, regulating immune homeostasis, and driving fibrotic responses. In SNH samples, LIGHT was highly expressed on macrophages, while its receptor HVEM was broadly expressed on hepatic macrophages, hepatocytes and epithelial cells respectively, suggesting widespread engagement of this immunostimulatory

pathway. These findings align with previous studies demonstrating that LIGHT-HVEM signalling contributes to excessive inflammation and tissue damage in autoimmune contexts^{64,65}. Notably, LIGHT signalling has been implicated as an activation signal to its receptor HVEM⁶⁶. In the context of SNH, where we observe accelerated liver damage and failure for regeneration and remodelling, the upregulation of LIGHT signalling may reflect a key pathogenic axis linking excessive and aberrant immune activation with hepatic tissue excessive necrosis. Moreover, LIGHT-HVEM interactions can amplify type I interferon responses and synergise with antiviral pathways. Considering the robust interferonstimulated gene expression as discussed previously from our findings and HERV activation observed in SNH livers, it is plausible that LIGHT contributes to sustaining or amplifying these antiviral immune response programs. This raises the possibility that the LIGHT pathway serves as a molecular bridge between viral trigger, immune cells crosstalk, and progressive tissue damage in SNH. The lack of expression of LIGHT in AIH compared with SNH liver disease highlights its potential as a diagnostic biomarker to distinguish between the clinically overlapping conditions. Moreover, given the pathogenic role of the LIGHT axis in other autoimmune disorders, our findings suggest that therapeutic targeting of LIGHT-HVEM interactions may represent a novel treatment strategy.

Our results support a model whereby hepatic macrophage-driven antiviral responses in SNH represent a key pathogenic axis distinct from classical AIH, potentially explaining the aggressive clinical course by aberrant immune activation, uncontrolled hepatocyte necrosis leading to liver failure observed in SNH patients. These findings provide a novel immunopathological framework for SNH, highlighting macrophages and their interferon response as potential promising targets for future therapeutic intervention to prevent liver transplantation for SNH patients. This study defines SNH liver disease as a unique spatial and transcriptional immune entity characterised by expanded hepatic macrophage populations with antiviral signatures, CD63 expression, altered and aberrant intercellular immune activation, and evidence of HERV exposure from liver tissue from an unknown

trigger. While AIH and SNH share some common features, we now reveal with a multi-OMICs approach that they are fundamentally distinct in their spatial immunobiology. These findings highlight the value of spatial transcriptomics in resolving the tissue context of autoimmune liver diseases and provide new insights into the drivers of immune activation in SN, with potential diagnostic and therapeutic implications.

Limitations and future directions

A limitation of this study is the use of archival explant liver samples, with no access to freshly collected explant liver, biopsies or peripheral blood, as patients were often incubated during hospital arrival thus unable to consent for use of fresh tissue. This precluded the possibility of performing additional experimental validations or functional assays. Furthermore, there are currently no representative mouse models for seronegative liver disease, which limits the ability to perform in vivo mechanistic studies. Despite these constraints, we leveraged precious explant human liver samples from SNH and AlH that are matched across all experimental platforms in this study. For the first time, we comprehensively applied spatial transcriptomics using both Visium and CosMx, integrated meta-transcriptomics and validated these findings using tissue protein expression confirmed in collaboration with a liver histopathologist. These analyses provide first ever valuable insights into the immunopathology of seronegative liver disease, which require liver transplantation in almost all cases. Future work may benefit from prospective collection of fresh samples with consent from family members and the development of suitable animal models to further advance understanding of disease mechanisms and potential diagnostic and therapeutic avenues for the health and well-being of these patients with discovery science.

DATA AVAILABILITY

Our CosMx spatial transcriptomics data are freely available for user-friendly interactive

browsing online (bham.ac.uk website in progress). All raw and processed sequencing data

for Visium and meta-transcriptomics work are deposited in ArrayExpress under accession

numbers E-MTAB-15851 and E-MTAB-15835 respectively. CosMx SMI raw and processed

data is available on BioImage Archive accession number S-BIAD2346. Lists of genes used

to identify cell subsets for analysis and clustering results are available as Supplementary

Tables provided with this paper.

CODE AVAILABILITY

All code is available on GitHub:

https://github.com/AmberBozward/SNH AIH spatial transcriptome

36

REFERENCES

- Bozward, A. G., Davies, S. P., Morris, S. M., Kayani, K. & Oo, Y. H. Cellular interactions in self-directed immune-mediated liver diseases. *J Hepatol* 82, 1110-1124 (2025). https://doi.org:10.1016/j.jhep.2025.01.002
- Gleeson, D. et al. British Society of Gastroenterology guidelines for diagnosis and management of autoimmune hepatitis. Gut 74, 1364-1409 (2025). https://doi.org:10.1136/gutjnl-2024-333171
- Oo, Y. H., Hubscher, S. G. & Adams, D. H. Autoimmune hepatitis: new paradigms in the pathogenesis, diagnosis, and management. *Hepatol Int* **4**, 475-493 (2010). https://doi.org:10.1007/s12072-010-9183-5
- 4 Czaja, A. J. Autoantibody-negative autoimmune hepatitis. *Dig Dis Sci* **57**, 610-624 (2012). https://doi.org:10.1007/s10620-011-2017-z
- Bhumi, S. A. & Wu, G. Y. Seronegative Autoimmune Hepatitis. *J Clin Transl Hepatol* 11, 459-465 (2023). https://doi.org:10.14218/JCTH.2022.00235
- 7 Lenti, M. V. et al. Seronegative autoimmune diseases: A challenging diagnosis.
 Autoimmun Rev 21, 103143 (2022). https://doi.org:10.1016/j.autrev.2022.103143
- 8 Krawitt, E. L. Autoimmune hepatitis. *N Engl J Med* **354**, 54-66 (2006). https://doi.org:10.1056/NEJMra050408
- Brahim, I., Brahim, I., Hazime, R. & Admou, B. [Autoimmune hepatitis: Immunological diagnosis]. *Presse Med* 46, 1008-1019 (2017).
 https://doi.org:10.1016/j.lpm.2017.08.012
- Donaghy, L. *et al.* Clinical and laboratory features and natural history of seronegative hepatitis in a nontransplant centre. *Eur J Gastroenterol Hepatol* **25**, 1159-1164 (2013). https://doi.org:10.1097/MEG.0b013e3283610484

- He, S. S. et al. High-plex imaging of RNA and proteins at subcellular resolution in fixed tissue by spatial molecular imaging. Nature Biotechnology 40 (2022). https://doi.org:10.1038/s41587-022-01483-z
- Hao, Y. et al. Integrated analysis of multimodal single-cell data. Cell 184, 3573-3587
 e3529 (2021). https://doi.org:10.1016/j.cell.2021.04.048
- Korsunsky, I. et al. Fast, sensitive and accurate integration of single-cell data with Harmony. Nat Methods 16, 1289-1296 (2019). https://doi.org:10.1038/s41592-019-0619-0
- Aran, D. et al. Reference-based analysis of lung single-cell sequencing reveals a transitional profibrotic macrophage. Nat Immunol 20, 163-172 (2019). https://doi.org:10.1038/s41590-018-0276-y
- MacParland, S. A. et al. Single cell RNA sequencing of human liver reveals distinct intrahepatic macrophage populations. Nat Commun 9, 4383 (2018).
 https://doi.org:10.1038/s41467-018-06318-7
- Newman, A. M. *et al.* Determining cell type abundance and expression from bulk tissues with digital cytometry. *Nat Biotechnol* **37**, 773-782 (2019). https://doi.org:10.1038/s41587-019-0114-2
- 17 Chung, B. K., Ogaard, J., Reims, H. M., Karlsen, T. H. & Melum, E. Spatial transcriptomics identifies enriched gene expression and cell types in human liver fibrosis. *Hepatol Commun* **6**, 2538-2550 (2022). https://doi.org:10.1002/hep4.2001
- Leek, J. T., Johnson, W. E., Parker, H. S., Jaffe, A. E. & Storey, J. D. The sva package for removing batch effects and other unwanted variation in high-throughput experiments. *Bioinformatics* 28, 882-883 (2012).
 https://doi.org:10.1093/bioinformatics/bts034
- Szklarczyk, D. et al. The STRING database in 2023: protein-protein association networks and functional enrichment analyses for any sequenced genome of interest. Nucleic Acids Res 51, D638-D646 (2023). https://doi.org:10.1093/nar/gkac1000

- Han, H. *et al.* TRRUST: a reference database of human transcriptional regulatory interactions. *Sci Rep* **5**, 11432 (2015). https://doi.org:10.1038/srep11432
- 21 Love, M. I., Huber, W. & Anders, S. Moderated estimation of fold change and dispersion for RNA-seq data with DESeq2. *Genome Biol* 15, 550 (2014). https://doi.org:10.1186/s13059-014-0550-8
- Palla, G. et al. Squidpy: a scalable framework for spatial omics analysis. *Nature Methods* **19**, 171-+ (2022). https://doi.org:10.1038/s41592-021-01358-2
- Baddeley, A., Rubak, E. & Turner, R. Spatial Point Patterns: Methodology and Applications with R. *Chap Hall Crc Interd*, 1-810 (2016).
- Davies, S. P. et al. Expression of E-cadherin by CD8(+) T cells promotes their invasion into biliary epithelial cells. *Nat Commun* **15**, 853 (2024).

 https://doi.org:10.1038/s41467-024-44910-2
- Davies, S. P. et al. Hepatocytes Delete Regulatory T Cells by Enclysis, a CD4(+) T Cell Engulfment Process. Cell Rep 29, 1610-1620 e1614 (2019).

 https://doi.org:10.1016/j.celrep.2019.09.068
- 26 Chen, S., Zhou, Y., Chen, Y. & Gu, J. fastp: an ultra-fast all-in-one FASTQ preprocessor. *Bioinformatics* 34, i884-i890 (2018).
 https://doi.org:10.1093/bioinformatics/bty560
- 27 Langmead, B. & Salzberg, S. L. Fast gapped-read alignment with Bowtie 2. *Nat Methods* **9**, 357-359 (2012). https://doi.org:10.1038/nmeth.1923
- Bendall, M. L. *et al.* Telescope: Characterization of the retrotranscriptome by accurate estimation of transposable element expression. *PLOS Computational Biology* **15**, e1006453 (2019). https://doi.org:10.1371/journal.pcbi.1006453
- 29 Patro, R., Duggal, G., Love, M. I., Irizarry, R. A. & Kingsford, C. Salmon provides fast and bias-aware quantification of transcript expression. *Nature Methods* 14, 417-419 (2017). https://doi.org:10.1038/nmeth.4197

- Love, M. I., Huber, W. & Anders, S. Moderated estimation of fold change and dispersion for RNA-seq data with DESeq2. *Genome Biology* **15**, 550 (2014). https://doi.org:10.1186/s13059-014-0550-8
- Song, Q. *et al.* Type I interferon signaling facilitates resolution of acute liver injury by priming macrophage polarization. *Cell Mol Immunol* **20**, 143-157 (2023). https://doi.org:10.1038/s41423-022-00966-y
- Borst, K. *et al.* Type I interferon receptor signaling delays Kupffer cell replenishment during acute fulminant viral hepatitis. *J Hepatol* **68**, 682-690 (2018). https://doi.org:10.1016/j.jhep.2017.11.029
- Verhelst, J., Parthoens, E., Schepens, B., Fiers, W. & Saelens, X. Interferon-inducible protein Mx1 inhibits influenza virus by interfering with functional viral ribonucleoprotein complex assembly. *J Virol* 86, 13445-13455 (2012). https://doi.org:10.1128/JVI.01682-12
- 34 Ivashkiv, L. B. & Donlin, L. T. Regulation of type I interferon responses. Nat Rev Immunol 14, 36-49 (2014). https://doi.org:10.1038/nri3581
- Wies, I. et al. Identification of target antigen for SLA/LP autoantibodies in autoimmune hepatitis. Lancet 355, 1510-1515 (2000). https://doi.org:10.1016/s0140-6736(00)02166-8
- Banchereau, J. & Pascual, V. Type I interferon in systemic lupus erythematosus and other autoimmune diseases. *Immunity* 25, 383-392 (2006).
 https://doi.org:10.1016/j.immuni.2006.08.010
- 37 Krenkel, O. & Tacke, F. Liver macrophages in tissue homeostasis and disease. *Nat Rev Immunol* **17**, 306-321 (2017). https://doi.org:10.1038/nri.2017.11
- Sigoillot, F. D., Berkowski, J. A., Sigoillot, S. M., Kotsis, D. H. & Guy, H. I. Cell cycle-dependent regulation of pyrimidine biosynthesis. *J Biol Chem* 278, 3403-3409 (2003). https://doi.org:10.1074/jbc.M211078200

- 39 Schmidt, L. E. & Dalhoff, K. Alpha-fetoprotein is a predictor of outcome in acetaminophen-induced liver injury. *Hepatology* 41, 26-31 (2005). https://doi.org:10.1002/hep.20511
- Bhushan, B. *et al.* Pro-regenerative signaling after acetaminophen-induced acute liver injury in mice identified using a novel incremental dose model. *Am J Pathol* **184**, 3013-3025 (2014). https://doi.org:10.1016/j.ajpath.2014.07.019
- 41 Pols, M. S. & Klumperman, J. Trafficking and function of the tetraspanin CD63. *Exp*Cell Res **315**, 1584-1592 (2009). https://doi.org:10.1016/j.yexcr.2008.09.020
- Beinert, T., Munzing, S., Possinger, K. & Krombach, F. Increased expression of the tetraspanins CD53 and CD63 on apoptotic human neutrophils. *J Leukoc Biol* **67**, 369-373 (2000). https://doi.org:10.1002/jlb.67.3.369
- Nail, H. M., Chiu, C. C., Leung, C. H., Ahmed, M. M. M. & Wang, H. D. Exosomal miRNA-mediated intercellular communications and immunomodulatory effects in tumor microenvironments. *J Biomed Sci* **30**, 69 (2023). https://doi.org:10.1186/s12929-023-00964-w
- Florin, L. & Lang, T. Tetraspanin Assemblies in Virus Infection. *Front Immunol* **9**, 1140 (2018). https://doi.org:10.3389/fimmu.2018.01140
- Spoden, G. *et al.* Clathrin- and caveolin-independent entry of human papillomavirus type 16--involvement of tetraspanin-enriched microdomains (TEMs). *PLoS One* **3**, e3313 (2008). https://doi.org:10.1371/journal.pone.0003313
- 46 Fu, E. et al. Tetraspanin CD63 is a regulator of HIV-1 replication. Int J Clin Exp Pathol8, 1184-1198 (2015).
- 47 Grassel, L. et al. The CD63-Syntenin-1 Complex Controls Post-Endocytic Trafficking of Oncogenic Human Papillomaviruses. Sci Rep 6, 32337 (2016).
 https://doi.org:10.1038/srep32337
- Karlas, A. et al. Genome-wide RNAi screen identifies human host factors crucial for influenza virus replication. Nature 463, 818-822 (2010).
 https://doi.org:10.1038/nature08760

- 49 Raaben, M. *et al.* NRP2 and CD63 Are Host Factors for Lujo Virus Cell Entry. *Cell Host Microbe* **22**, 688-696 e685 (2017). https://doi.org:10.1016/j.chom.2017.10.002
- Takawale, A. et al. Tissue Inhibitor of Matrix Metalloproteinase-1 Promotes
 Myocardial Fibrosis by Mediating CD63-Integrin beta1 Interaction. Hypertension 69,
 1092-1103 (2017). https://doi.org:10.1161/HYPERTENSIONAHA.117.09045
- Alvarez, F. et al. International Autoimmune Hepatitis Group Report: review of criteria for diagnosis of autoimmune hepatitis. *J Hepatol* **31**, 929-938 (1999). https://doi.org:10.1016/s0168-8278(99)80297-9
- Boberg, K. M. *et al.* Overlap syndromes: the International Autoimmune Hepatitis Group (IAIHG) position statement on a controversial issue. *J Hepatol* **54**, 374-385 (2011). https://doi.org:10.1016/j.jhep.2010.09.002
- Johnson, P. J. & McFarlane, I. G. Meeting report: International Autoimmune Hepatitis Group. *Hepatology* **18**, 998-1005 (1993). https://doi.org:10.1002/hep.1840180435
- Nexo, B. A. *et al.* Are human endogenous retroviruses triggers of autoimmune diseases? Unveiling associations of three diseases and viral loci. *Immunol Res* **64**, 55-63 (2016). https://doi.org:10.1007/s12026-015-8671-z
- Tai, A. K. et al. Human endogenous retrovirus-K18 Env as a risk factor in multiple sclerosis. Mult Scler 14, 1175-1180 (2008).

 https://doi.org:10.1177/1352458508094641
- Manghera, M. & Douville, R. N. Endogenous retrovirus-K promoter: a landing strip for inflammatory transcription factors? *Retrovirology* 10, 16 (2013).
 https://doi.org:10.1186/1742-4690-10-16
- 57 Laderach, F. *et al.* EBV induces CNS homing of B cells attracting inflammatory T cells. *Nature* **646**, 171-179 (2025). https://doi.org:10.1038/s41586-025-09378-0
- Franke, A. et al. Genome-wide association study for ulcerative colitis identifies risk loci at 7q22 and 22q13 (IL17REL). Nat Genet 42, 292-294 (2010). https://doi.org:10.1038/ng.553

- Franke, A. *et al.* Genome-wide meta-analysis increases to 71 the number of confirmed Crohn's disease susceptibility loci. *Nat Genet* **42**, 1118-1125 (2010). https://doi.org:10.1038/ng.717
- Hom, G. et al. Association of systemic lupus erythematosus with C8orf13-BLK and ITGAM-ITGAX. N Engl J Med 358, 900-909 (2008).
 https://doi.org:10.1056/NEJMoa0707865
- Gateva, V. et al. A large-scale replication study identifies TNIP1, PRDM1, JAZF1, UHRF1BP1 and IL10 as risk loci for systemic lupus erythematosus. *Nat Genet* 41, 1228-1233 (2009). https://doi.org:10.1038/ng.468
- Mieli-Vergani, G. et al. Autoimmune hepatitis. Nat Rev Dis Primers 4, 18017 (2018). https://doi.org:10.1038/nrdp.2018.17
- Ariza, M. E. & Williams, M. V. A human endogenous retrovirus K dUTPase triggers a TH1, TH17 cytokine response: does it have a role in psoriasis? *J Invest Dermatol* 131, 2419-2427 (2011). https://doi.org:10.1038/jid.2011.217
- Gupta, R. K. *et al.* LIGHT signaling through LTbetaR and HVEM in keratinocytes promotes psoriasis and atopic dermatitis-like skin inflammation. *J Autoimmun* **144**, 103177 (2024). https://doi.org:10.1016/j.jaut.2024.103177
- Sakoda, Y. *et al.* Pathogenic Function of Herpesvirus Entry Mediator in Experimental Autoimmune Uveitis by Induction of Th1- and Th17-Type T Cell Responses. *J Immunol* **196**, 2947-2954 (2016). https://doi.org:10.4049/jimmunol.1501742
- Ware, C. F. Targeting the LIGHT-HVEM pathway. *Adv Exp Med Biol* **647**, 146-155 (2009). https://doi.org:10.1007/978-0-387-89520-8_10

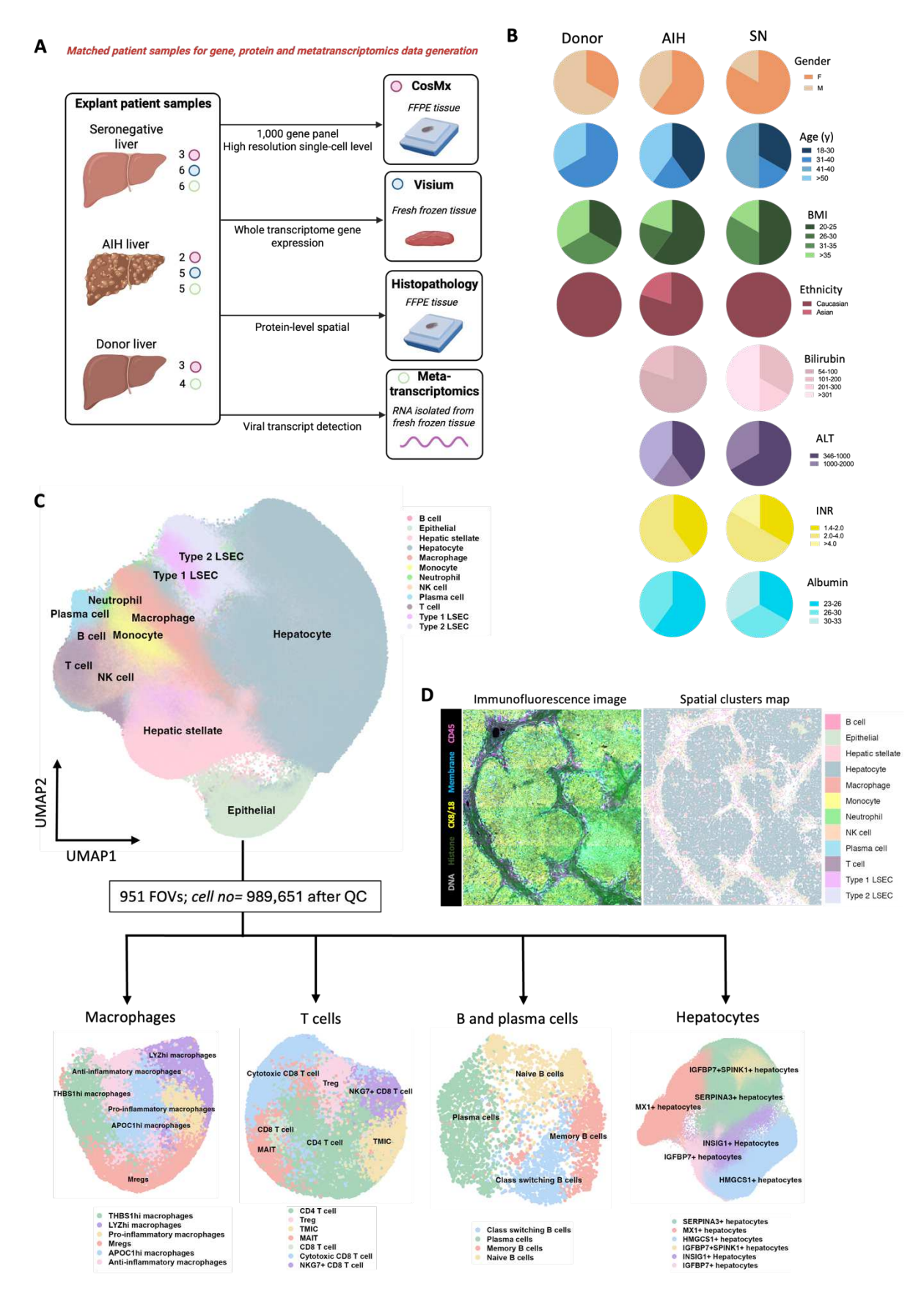


Fig.1| Overview of study design, patient samples, clinical features and spatial cell type mapping.

A An outline of the samples collected and used for various methods throughout the study. **B** Clinical characteristics of patients included in the spatial transcriptomics work from Autoimmune hepatitis (AIH), seronegative hepatitis liver disease (SN) and donor control (D) explant liver samples. **C** CosMx cell types identified at a broad resolution outlining the number of high-quality transcriptomes (989,651 cells) and fine resolution cell subsets of Macrophages, T cells, B cells and Hepatocytes from all samples combined. **D** Cell types identified using the gene signatures viewed spatially and the stained immunofluorescence image for DNA, histone, membrane, CK8/18 and CD45.

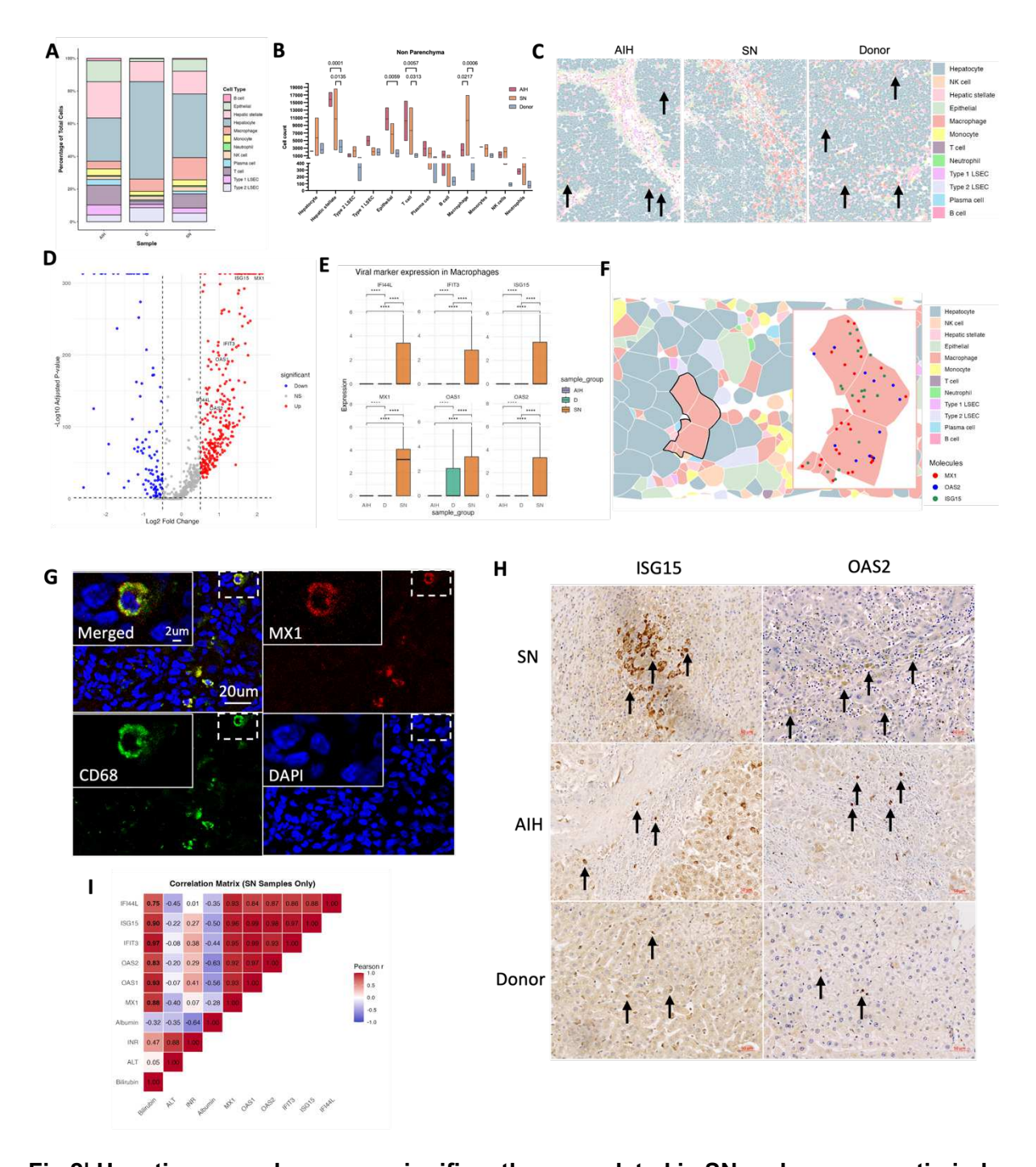


Fig.2| Hepatic macrophages are significantly upregulated in SN and express anti-viral markers.

A-F CosMx 1k-plex panel using Autoimmune hepatitis (AIH), seronegative hepatitis liver disease (SN) and donor control (D) samples. **A** Stacked bar plot showing the relative abundance of annotated cell types in samples from AIH, SN and D samples. Each bar represents the percentage contribution of each cell type to the total cell population within a sample. **B** Areas of parenchyma and non-parenchyma were spatially differentiated for each

sample and combined to determine cell abundances for each cohort. Cell counts for areas of non-parenchyma were plotted and compared between AIH, SN and D cohorts using (Mann-Whitney test), C Representative spatial transcriptomics images showing the distribution of cell types between AIH, SN and D samples each colour represents a different cell type. D Volcano plot comparing markers upregulated on macrophages in SN samples compared to macrophages in AIH samples. Highlighting significantly upregulated anti-viral associated markers. E Comparison of anti-viral markers IFI44L, IFIT3, ISG15, MX1, OAS1 and OAS2 between AIH, SN and D samples using Mann-Whitney test. F Representative CosMx spatial transcriptomics map showing segmented cells coloured by annotated cell type. A selected macrophage region (black outline) is enlarged to display single-molecule resolution of transcripts for MX1 (red), OAS2 (blue) and ISG15 (green) on SN liver tissue. G Immunoflourescence images showing the expression of MX1 (yellow) on seronegative liver disease, using the same tissue samples profiled with CosMx. Macrophages are denoted by CD68 (Green) and DAPI (blue) staining. H Immunohistochemistry staining of ISG15 and OAS2 (brown) in explant liver tissue from SN, AIH and donor samples, performed on the same samples profiled with CosMx analysis. I Pearson correlation coefficients (r) between clinical parameters (bilirubin, ALT, INR and albumin) and anti-viral associated genes (IFI44L, IFIT3, ISG15, MX1, OAS1 and OAS2) in SN liver samples. Positive correlations are shown in red and negative correlations in blue, with intensity reflecting correlation strength.

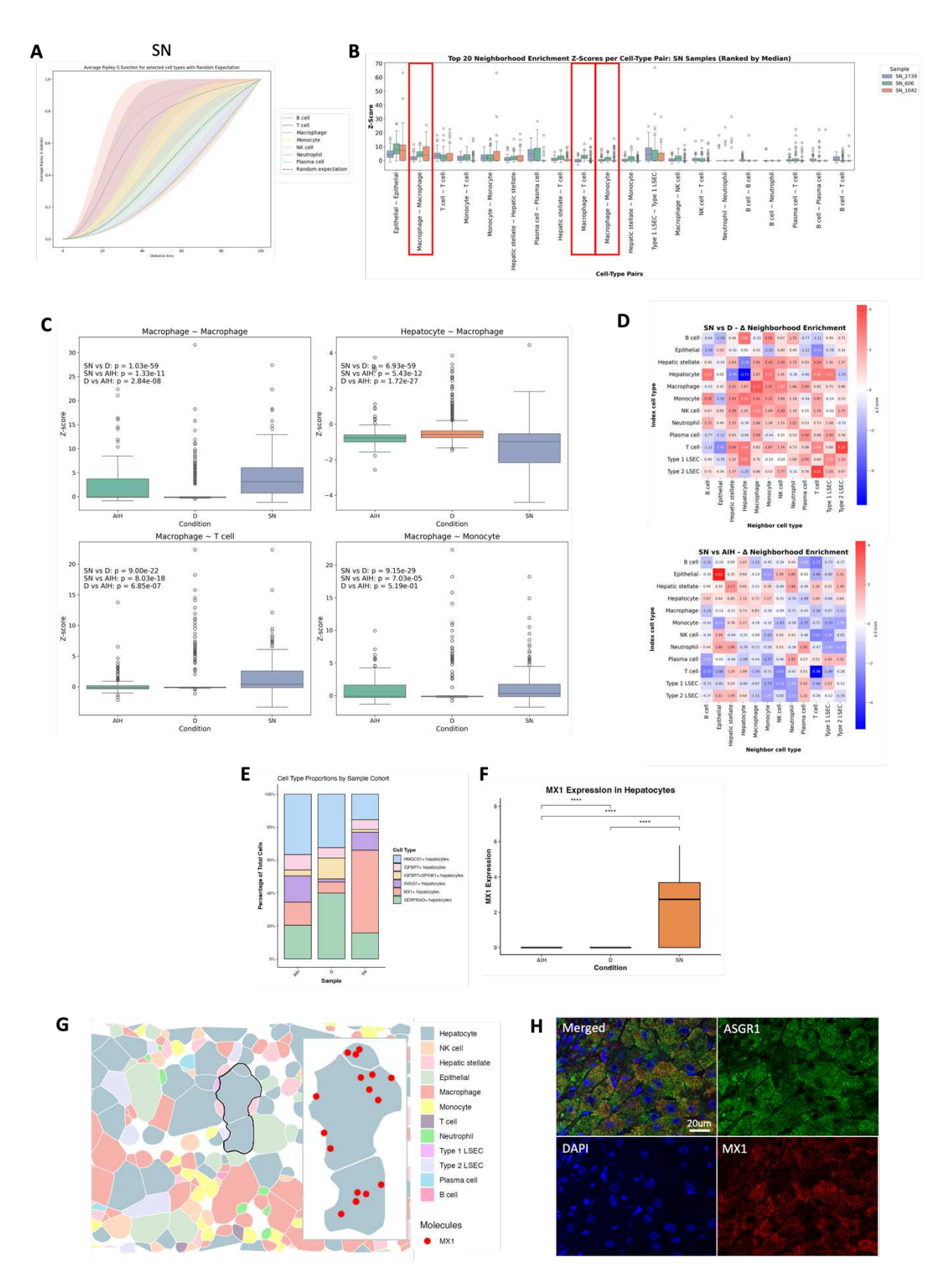


Fig.3| Spatial clustering and neighbourhood enrichment of immune and parenchymal cells in seronegative (SN), autoimmune hepatitis (AIH) and donor (D) liver tissue.

Hepatocyte antiviral responses and immune cell composition in SN liver disease.

A Average Ripley's G function for selected immune cells types compared with random expectation, demonstrating significant clustering across SN liver samples. Shaded areas represent variability across samples. B Top 20 neighbourhood enrichment Z-scores for cellcell clustering localisation in SN samples, ranked by median value across patients. Red boxes highlight macrophage-macrophage, macrophage-T cells and macrophage-monocyte co-localisations. C Boxplot showing neighbourhood enrichment Z-scores for selected cellcell interactions across conditions (SN, AIH, D). Significant differences (Mann Whitney test) are indicated on each plot. **D** Heatmaps of differential neighbourhood enrichment (Δ Z-score) comparing SN with donor (left) and SN with AIH (right). Positive values (Red) indicate increased enrichment in SN, while negative values (blue) indicate reduced colocalization relative to the comparator group. E Stacked bar plot showing the proportions of hepatocyte subpopulations across conditions (AIH, D, SN). F Boxplot of MX1 expression in hepatocytes across conditions, demonstrating significant upregulation in SN. G Representative CosMx spatial transcriptomics map showing segmented cells coloured by annotated cell type. A selected hepatocyte region (black outline) is enlarged to display single-molecule resolution of transcripts for MX1 (red) on SN liver tissue. H Immunoflourescence images showing the distribution of expression of MX1 (red) in seronegative liver disease, using the same tissue samples profiled with CosMx. Hepatocytes are denoted by asialoglycoprotein receptor (ASGR1; green) and DAPI (blue) staining.

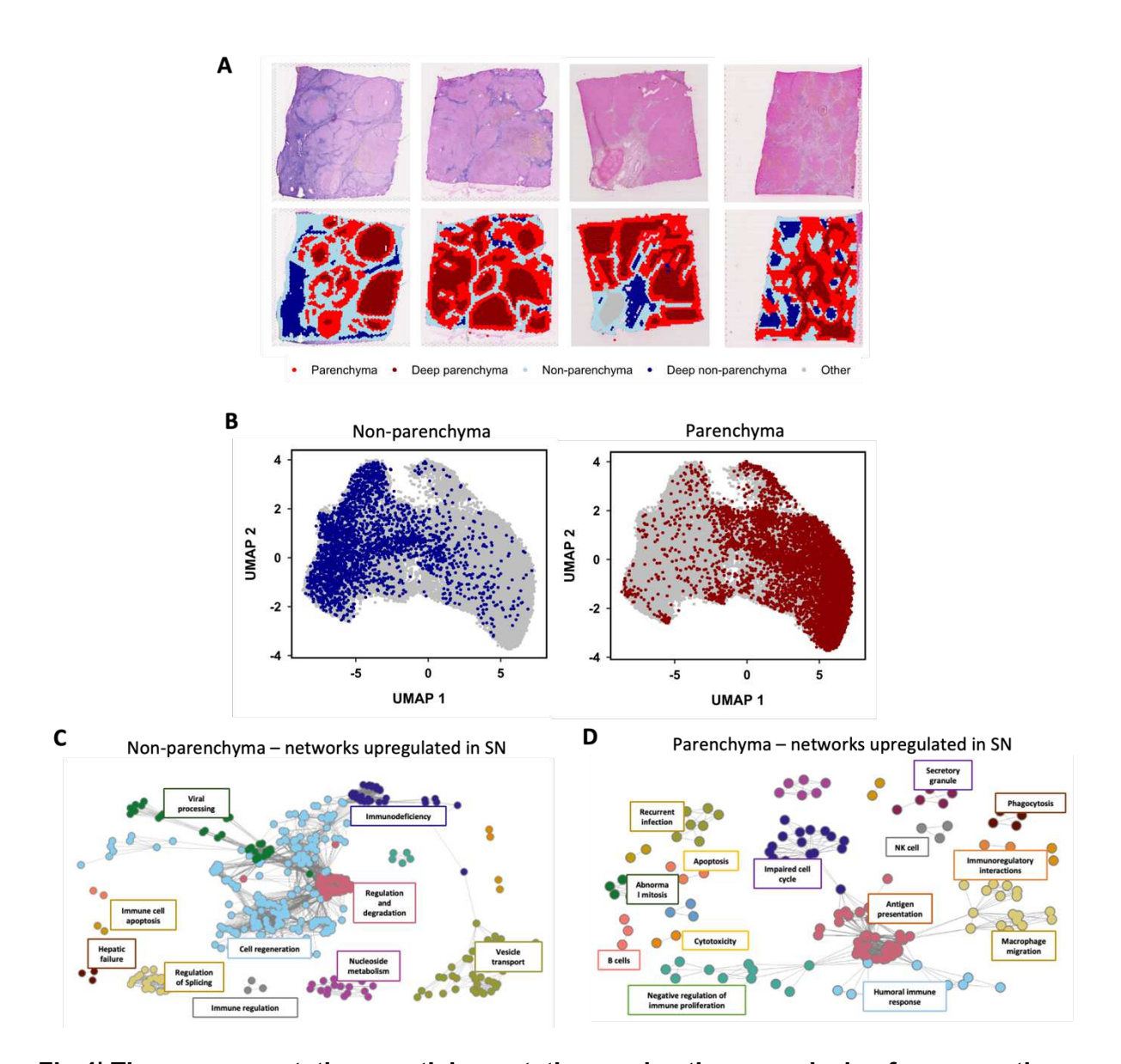


Fig.4| Tissue segmentation, spatial annotation, and pathway analysis of seronegative hepatitis and autoimmune hepatitis explant liver tissue.

A Representative H&E-stained explant liver sections with corresponding computational segmentation in parenchyma (red), deep parenchyma (dark red), non-parenchyma (blue), deep non-parenchyma (dark blue), and other tissue regions (grey). B UMAP projections showing separation of parenchymal (red) and non-parenchymal (blue) compartments across all samples. C-D Functional network analysis of differentially expressed genes between C non-parenchyma and D parenchyma compartments. Networks are annotated with enriched biological processes.

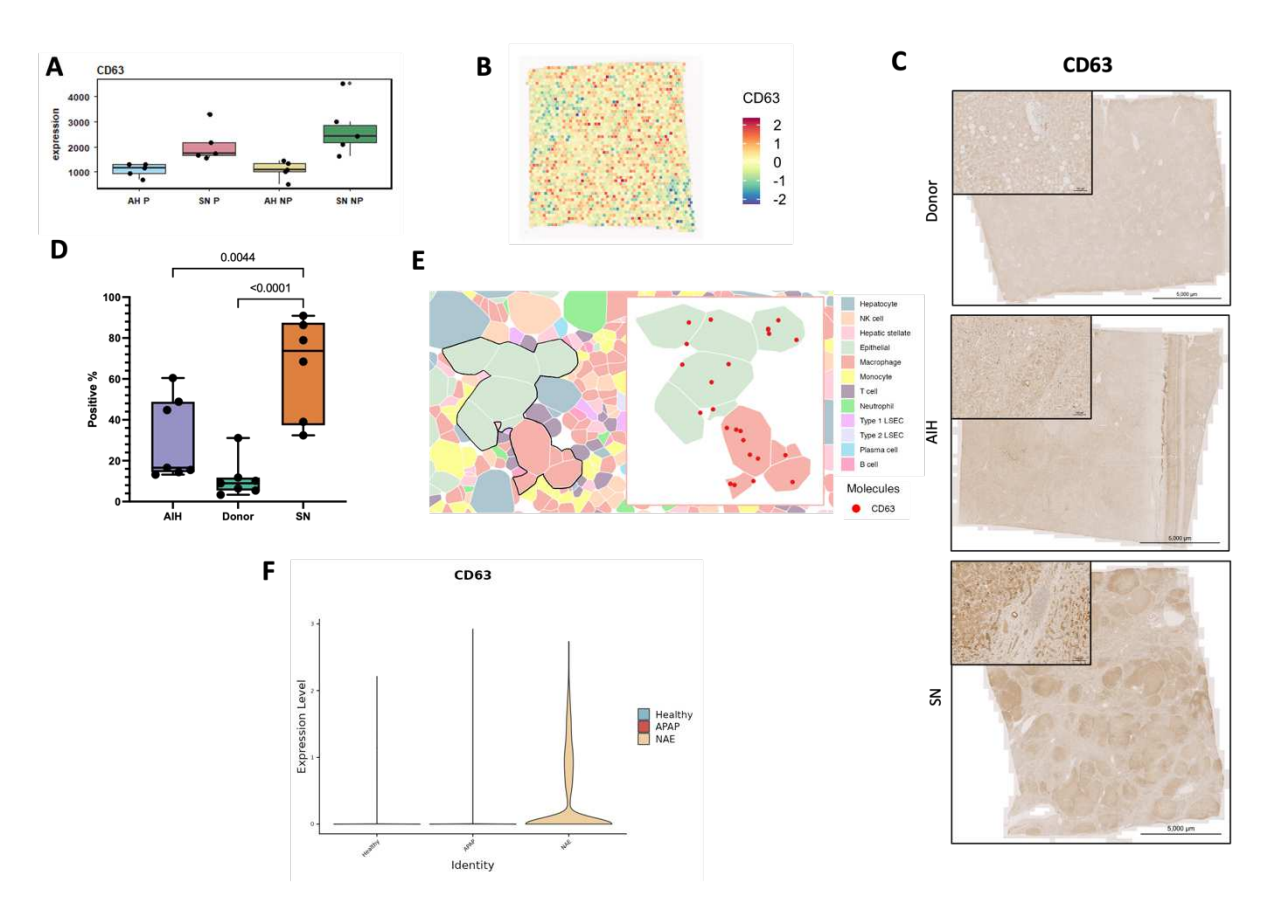


Fig.5| CD63 expression is enriched in seronegative liver disease.

A Boxplot showing increased CD63 expression in parenchymal and non-parenchymal areas of patients with SN liver disease compared to lower expression in AlH samples. **B** Visium spatial transcriptomics visualisation showing CD63 expression distribution across a SN liver tissue sample. **C** Immunohistochemistry staining of CD63 (brown) in explant liver tissue from Donor (*top*), AlH (middle) and SN (*bottom*) samples, performed on the same samples profiled with spatial transcriptomics analysis. **D** Boxplot quantifying the expression of CD63 stained using immunohistochemistry on AlH, donor and SN FFPE matched liver samples (Mann Whitney test). **E** Representative CosMx spatial transcriptomics map showing segmented cells coloured by annotated cell type. A selected macrophage region (black outline) is enlarged to display single-molecule resolution of transcripts for CD63 (red) on SN liver tissue. **F** Violin plot showing the expression of CD63 on mononuclear phagocytes in healthy control, acetaminophen (APAP) and NAE liver samples from a publicly available scRNAseq dataset (https://shiny.igc.ed.ac.uk/7efa5350ba94425388e47ea7cdd5aa64/).

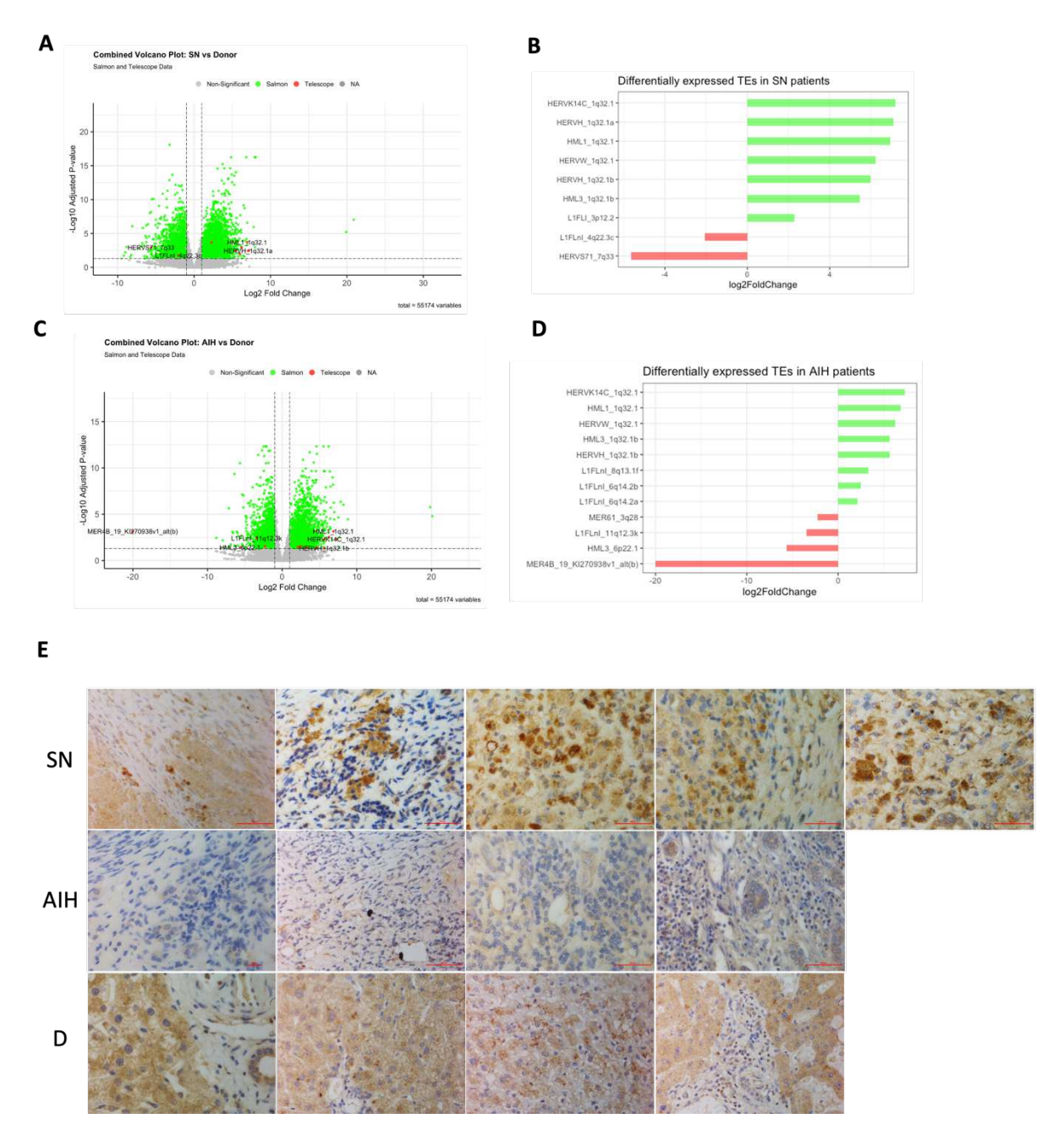


Fig.6| Seronegative liver disease patient samples contain HERV virus.

A Volcano Plot of the comparison AIH vs. donors. Red points are differentially expressed transposable element quantified by Telescope and green points are differentially expressed genes quantified by Salmon. B Differentially expressed transposable element in SN patients quantified by Telescope. C Volcano Plot of the comparison AIH vs. donors. Red points are differentially expressed transposable element quantified by Telescope and green points are differentially expressed genes quantified by Salmon. D Differentially expressed transposable element in AIH patients quantified by Telescope. E Immunohistochemistry staining of HERV

(brown) in explant liver tissue from SN (*top*), AIH (*middle*) and donor (*bottom*) samples, performed on the same samples profiled with spatial transcriptomics analysis.

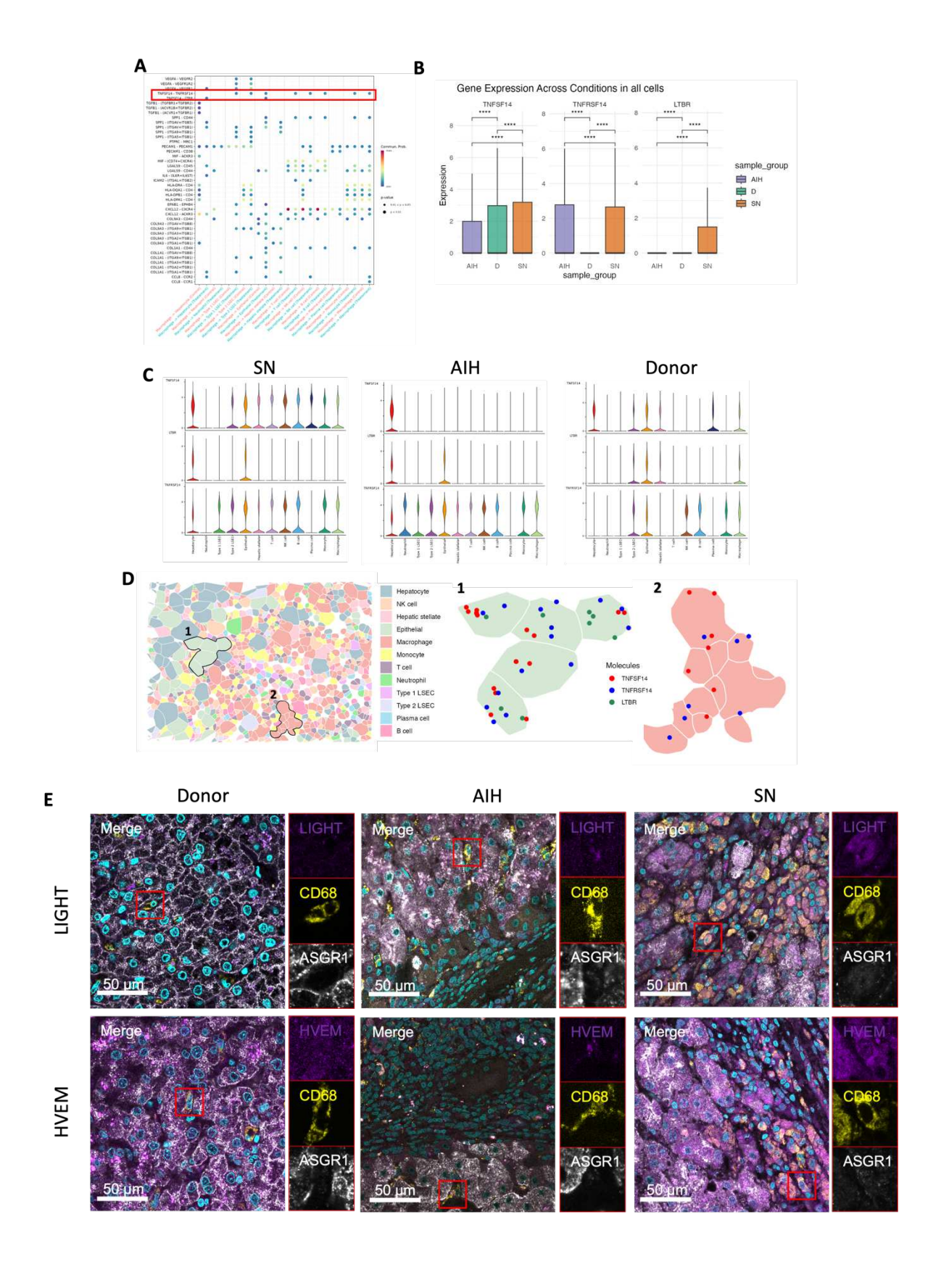


Fig.7| LIGHT pathway signalling is upregulated in seronegative liver disease and enriched in macrophages.

A CellChat analysis of ligand-receptor interactions outgoing from macrophages to all other cell types comparing between SN and donor samples in non-parenchymal areas. The red outline highlights the LIGHT pathway interactions. **B** Comparison of LIGHT pathway markers TNFSF14, TNFRSF14 and LTBR between AIH, SN and D samples using Mann-Whitney test. C Cell-type resolved violin plots of TNFSF14, TNFRSF14 and LTBR expression across liver cell populations in SN (left), AIH (middle) and donor (right) samples. D Representative CosMx spatial transcriptomics map showing segmented cells coloured by annotated cell type. Two selected regions (black outline) highlighting areas of 1) epithelial cells and 2) macrophages are enlarged to display single-molecule resolution of transcripts for TNFSF14 (red), TNFRSF14 (blue) and LTBR (green) on SN liver tissue. E Immunofluorescence images showing the distribution of tumor necrosis factor superfamily member 14 (TNFSF14/LIGHT), Herpesvirus entry mediator (HVEM) and Lymphotoxin β receptor (LTβR; magenta) in liver tissues from non-cirrhotic donor livers (left) or explants livers from patients with seropositive autoimmune hepatitis (AIH; middle) or seronegative liver disease (SN; right). Hepatocytes and macrophages are denoted by asialoglycoprotein receptor (ASGR1; grey) and CD68 (yellow) staining, respectively.

Supplementary Files

This is a list of supplementary files associated with this preprint. Click to download.

- SupplementaryTable1.csv
- SupplementaryTable2.csv
- SupplementaryTable3.csv
- SupplementaryTable4.xlsx
- SupplementaryTable5.xlsx
- Dataaccessioncodes.pdf
- ReportingSummary.pdf
- Supplementarymaterial.docx